

Weak-Strong Simulation Studies for the LHC Long-Range Beam-Beam Compensation

F. Zimmermann, CERN, Geneva, Switzerland

Abstract

Using weak-strong computer simulations, we study the improvement of LHC tune footprints and dynamic aperture by electromagnetic lenses, *i.e.*, pulsed wires, which compensate for the long-range beam-beam interaction. In particular, we explore the robustness of this compensation scheme to linear optics imperfections as well as to errors in wire strength and position.

1 INTRODUCTION

The long-range or parasitic collisions are expected to limit the dynamic aperture of the LHC [1, 2, 3]. A compensation scheme for the effect of the long-range collisions, proposed by J.-P. Koutchouk, is presently under investigation at CERN [4, 5, 6]. The compensation employs an electric wire on each side of each interaction point (IP). The wire carries an integrated current of about 80 Ampere meter, and it is placed at a horizontal or vertical distance from the beam that equals the effective beam-beam separation at the long-range encounters, about 9.5σ at top energy. If the current is pulsed or ramped at the start of each bunch train the correction can work even for the so-called PACMAN bunches [7], *i.e.*, for bunches which do not experience the full set of long-range encounters, due to gaps in the opposing beam.

In this report, we report weak-strong simulation results for the wire compensation scheme. The simulation program is the same as described in Ref. [2], except that two electric wires have been added. Considering two head-on collisions with alternating crossing and the parasitic collisions around each head-on IP, the simulation yields the tune footprints and the action diffusion rate at various betatron amplitudes. Using this simulation, we study the sensitivity of the wire compensation to various errors, such as to errors in the wire position, the wire strength, or the betatron phase advance between the wire and the collision point.

Section 2 describes the simulation model in more detail. Results are presented in Section 3. Conclusions are drawn in Section 4.

2 MODEL

The simulation study follows John Irwin's approach for the SSC [2, 8]. It is a 4-dimensional code, without synchrotron oscillations. However, tune modulation can be included as an option.

We consider two IPs, one with horizontal crossing, the other with vertical. This models the two main IPs in the

Table 1: Parameters.

parameter	symbol	value
number of particles per bunch	N_b	1.1×10^{11}
beam energy	E_b	7 TeV
rms beam size at IP	$\sigma_{x,y}^*$	$16 \mu\text{m}$
rms divergence at IP	$\theta_{x,y}^*$	$31.7 \mu\text{rad}$
IP beta function	$\beta_{x,y}^*$	50 cm
full crossing angle	θ_c	$300 \mu\text{rad}$
number of main collision points	n_{IP}	2
parasitic collisions per side	n_{par}	16
bunch spacing	L_{sep}	7.48 m
beam-beam parameter	ξ	0.00342
revolution frequency	f_{rev}	11.25 kHz

LHC. Simulation parameters are summarized in Table 1. At the parasitic collision points the beams are separated by $\theta_c/\theta_{x,y}^* \approx 9.5$ rms beam sizes. The fractional tunes are set to the LHC design values of 0.31 and 0.32. The phase advance between IPs is taken to be exactly half the total phase advance per turn.

At each IP we apply a series of 3 kicks representing, respectively,

- the lumped effect of long-range collisions and wire compensation on the incoming side,
- a head-on collision,
- the lumped effect of long-range collisions and wire compensation on the outgoing side.

2.1 Head-On Collision

The head-on collision with a round Gaussian beam is parametrized as

$$\Delta x' = \frac{2r_p N_b}{\gamma} \frac{x}{r^2} \left(1 - e^{-\frac{x^2}{2\sigma^{*2}}} \right) \quad (1)$$

$$\Delta y' = \frac{2r_p N_b}{\gamma} \frac{y}{r^2} \left(1 - e^{-\frac{y^2}{2\sigma^{*2}}} \right) \quad (2)$$

where $\sigma^* \equiv \sigma_x = \sigma_y$; $r = \sqrt{x^2 + y^2}$ is the radial distance to the origin, r_p the classical proton radius, γ the Lorentz factor, and N_b the bunch population. The phase-space coordinates x , x' , y , and y' refer to the IP.

2.2 Long-Range Interactions

All parasitic collisions (n_{par}) on one side of the IP are lumped into a single deflection. Assuming a perfect $\pi/2$

distance in phase advance between head-on and parasitic collision points, the kick is approximately expressed as a change in the IP coordinate (while the IP angle stays unchanged). For the IP with horizontal crossing, the IP coordinates and slopes are changed according to

$$\Delta x = n_{\text{par}} \frac{2r_p N_b}{\gamma} \left[\frac{x' + \theta_c}{\theta_t^2} \left(1 - e^{-\frac{\theta_t^2}{2\theta^{*2}}} \right) - \frac{1}{\theta_c} \left(1 - e^{-\frac{\theta_t^2}{2\theta^{*2}}} \right) \right] \quad (3)$$

$$\Delta y = n_{\text{par}} \frac{2r_p N_b}{\gamma} \frac{y'}{\theta_t^2} \left(1 - e^{-\frac{\theta_t^2}{2\theta^{*2}}} \right) \quad (4)$$

where

$$\theta_t \equiv ((x' + \theta_c)^2 + y'^2)^{1/2} \quad (5)$$

and $\theta^* \equiv \theta_x^* = \theta_y^*$ is the rms IP beam divergence. At the LHC, the effective number of parasitic crossings per side is $n_{\text{par}} \approx 16$. The expression for the kick is the same on both sides of the IP. The second IP, with vertical crossing, is treated analogously.

2.3 Wire Compensation

The new feature of the code is the electric wire. For a horizontal crossing, the effect of a thin wire is represented as:

$$\begin{aligned} \Delta x &= \frac{\mu_0 I_w l_w}{2\pi(B\rho)} \left[\frac{x' + \theta_{c,w} \pm \phi_x x / \beta_x^*}{\theta_{tw}^2} - \frac{1}{\theta_{c,w}} \right] \quad (6) \\ \Delta x' &= -(\pm 1) \phi_x \Delta x / \beta_x^* \\ \Delta y &= \frac{\mu_0 I_w l_w}{2\pi(B\rho)} \frac{y' \pm \phi_y y / \beta_y^*}{\theta_{tw}^2} \\ \Delta y' &= -(\pm 1) \phi_y \Delta y / \beta_y^* \end{aligned}$$

where

$$\theta_{tw} \equiv ((x' + \theta_{c,w} \pm \phi_x x / \beta_x^*)^2 + (y \pm \phi_y y / \beta_y^*)^2)^{1/2}, \quad (7)$$

and l_w is the length of the wire, $\theta_{c,w}$ is the angle at the IP representing the transverse distance between the beam and the wire, I_w the wire current, and $(B\rho)$ the magnetic rigidity of the beam. The \pm signs refer to the two sides of the IP. Again the vertical crossing is treated in analogy. The errors ϕ_x and ϕ_y represent the deviation in phase advance from the IP with respect to the ideal value $\pi/2$. Simultaneously they also give the differences in phase advance from the location of the long-range collisions. At the wire location presently contemplated, the phase errors are about $2-3^\circ$ in the design optics [4]. For perfect compensation, the wire current must be chosen as

$$I_w = -4\pi(B\rho)N_b r_p n_{\text{par}} / (\mu_0 \gamma l_w). \quad (8)$$

The ideal distance between wire and beam is $d_w \approx (\theta_c / \theta_{x,y}^*) \sigma$, where σ denotes the rms beam size at the wire. This corresponds to $\theta_{c,w} = \theta_c$.

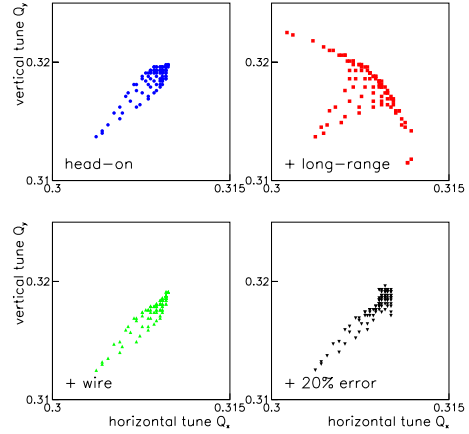


Figure 1: Tune footprints for various cases, for initial horizontal and vertical amplitudes extending to $7\sigma_{x,y}$. Top left: head-on collisions only; top right: head-on plus long-range collisions; bottom left: head-on plus long-range collisions and a perfect wire; bottom right: head-on plus long-range collisions and a wire with 20% strength error.

2.4 Compensation Errors

We consider five types of errors, namely,

- a simultaneous symmetric betatron phase error $\phi_{x,y}$ on both sides of each IP,
- a static wire strength error,
- a random wire strength error,
- a wire position error,
- a betatron phase error $\phi_{x,y}$ with only one wire per IP.

Simulation results for each case are discussed next.

3 RESULTS

Figure 1 shows tune footprints computed for initial amplitudes extending to $7\sigma_{x,y}$. The tunes were calculated by applying a fast Fourier transform to particle positions sampled over 4096 turns. The top left picture shows the tune footprint for the two head-on collisions alone, the top right the enhancement of the footprint by the long-range collisions. The bottom left picture demonstrates that an ideal wire reduces the footprint to a size equal to or even smaller than that for head-on collisions only. The compensation still works even with a significant static strength error, as illustrated in the last picture.

Diffusion rates are calculated by launching groups of 100 particles at identical start amplitudes in the horizontal and vertical plane, but with random initial betatron phase. The spread in linear action values is averaged over 1000 consecutive turns to reduce fluctuations due to regular

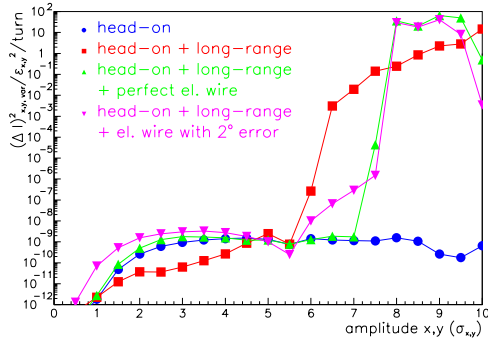


Figure 2: The diffusion per turn as a function of the start amplitude. Different cases are compared.

phase deformations, and to more clearly pronounce chaotic behavior. The mean increase per turn in the action variance measures the strength of the diffusion.

Figure 2 shows the simulated diffusion rates as a function of start amplitude. The vertical axis is on a logarithmic scale. It represents the increase in the action variance per turn, in units of the rms design emittance. Any value larger than 10^{-8} could indicate a significant diffusion over 10^8 turns. It is most noteworthy, that at an amplitude of about 6σ the diffusion rate increases by 7–9 orders of magnitude, if long-range collisions are present (the red curve, squares). The strong diffusion is absent when only head-on collisions are accounted for (the blue curve, circles). This is consistent with the results of Ref. [2]. When the electric compensating wire is added (green curve, upright triangles), the amplitude of the steep increase moves outwards by $1.5\text{--}2\sigma$, to about $7.5\text{--}8\sigma$. This remarkable improvement confirms the efficiency of the wire. Even with an imperfect wire (2° phase error - the pink curve, inverse triangles), the diffusion rates in the intermediate amplitude range $6\text{--}8\sigma$ is still several orders of magnitude lower than without the wire. Note that a 2σ improvement of the dynamic aperture, in both planes, might greatly improve the operating margin of the LHC.

That the wire compensation fails for amplitudes larger than 8σ is understandable. At amplitudes above 8σ the particles start passing through the core of the opposing beam, where the beam force strongly deviates from the $1/r$ force of the wire.

Figure 3 shows a more systematic study of the effect of a phase error. The same phase error with respect to the head-on collision point was assumed for the wires on either side of the IP and in both planes. Results are compared for three different amplitudes. Since, for phase errors of about $\pm 10^\circ$, the diffusion rate at 7.5σ increases to the uncompensated level, we may consider this value as the phase tolerance. In practice, the phase errors are confined to less than $2 \pm 1^\circ$ [4], *i.e.*, phase errors due to optical imperfections will have a negligible effect on the beam-beam compensa-

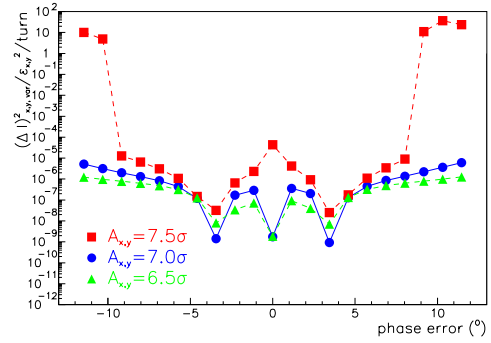


Figure 3: Variation of diffusion rate with symmetric betatron phase error at various amplitudes. The phase errors for the wires on either side and for the two planes are all assumed to be equal.

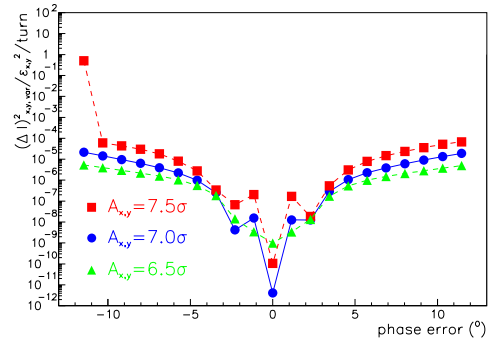


Figure 4: Variation of diffusion rate with betatron phase error at various amplitudes, if there is a compensating wire only on one side of each IP.

tion.

Alternatively, we consider the case that there is only one wire per IP and study the sensitivity to betatron phase errors in this configuration. The results are shown in Fig. 4. They are similar to, or even lower than, those in Fig. 3, despite of the reduced symmetry. Since it is not possible to choose a location with a phase error less than 1° also here we take $\pm 10^\circ$ as the tolerance. The differences in the diffusion rates for one and two wires depend on the working point.

If the wire current is not perfect, the compensation degrades. This is studied in Fig. 5 (again for two wires per IP), depicting diffusion rates at 6.5 , 7 and 7.5σ as a function of the wire strength error in percent. Especially at the largest amplitude, the dependence is rather erratic, presumably indicating the existence of resonance islands. Static strength errors in the range between 0 and -10% appear acceptable.

The effect of a random change in the wire strength from turn to turn is illustrated in Figs. 6 and 7. The strength of

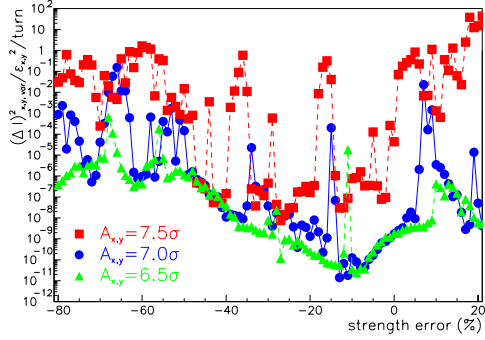


Figure 5: Variation of diffusion rate with static wire strength error (in units of percent) at various amplitudes.

each wire is assumed to fluctuate from turn to turn. Plotted along the horizontal axis is the normalized peak value $\Delta I_w/I_w$ of the random fluctuation in wire current. The latter is uniformly distributed between $-\Delta I_w$ and ΔI_w . Then the diffusion rates should be symmetric around zero, and deviations from the mirror symmetry reflect the uncertainty of the simulation result, due to the choice of random seed.

In the simulation of Fig. 6, we have assumed that the fluctuation in wire strength does not give rise to dipolar deflections. This means, that in Eq. (6) all three terms containing the factor $\theta_{c,w}$ were varied simultaneously. For the corresponding results in Fig. 7, only the average dipole deflection, *i.e.*, not including the fluctuating part, was subtracted from the wire force. In this case, the beam experiences random dipole kicks in addition to fluctuating focusing forces, and higher order terms. Since no fast orbit feedback is foreseen for the LHC at top energy the second simulation is more realistic. The difference in the computed diffusion rates is small, however, which suggests that the random quadrupolar excitation is more harmful than the dipolar one. Both figures indicate that the tolerance on the turn-to-turn stability of the wire is less than 0.1%.

Finally, Fig. 8 shows simulated diffusion rates as a function of an error in the transverse distance between beam and wire. We observe that errors in the wire position towards larger amplitudes are preferred, presumably because the $1/r$ field increases strongly in the vicinity of the thin wire. Note that the sharp increase in the diffusion rates for smaller distances is consistent with the steep rise at an amplitude of 7.5σ , in Fig. 2, and that the preservation of a low diffusion rate for distances 10–20% larger than nominal is compatible with the dependence on the static strength error in Fig. 5. We deduce from Fig. 8 that the tolerable range of distances extends approximately between 0 and 20% of the optimum distance.

In LHC operation, the relative distance of beam and wire can be determined with sufficient precision by detecting the effect of the wire current on the closed orbit.

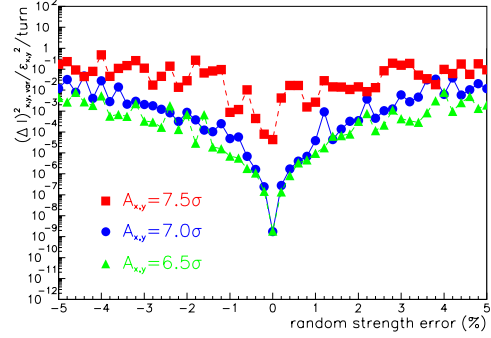


Figure 6: Variation of diffusion rate with peak value of turn-to-turn random wire strength error at various amplitudes. The dipolar deflection by the wire is subtracted including its fluctuation.

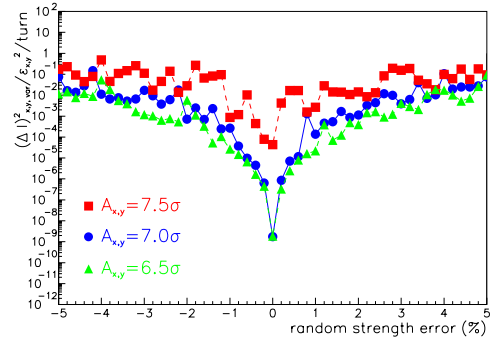


Figure 7: Variation of diffusion rate with random wire strength error at various amplitudes. The average dipole deflection is subtracted.

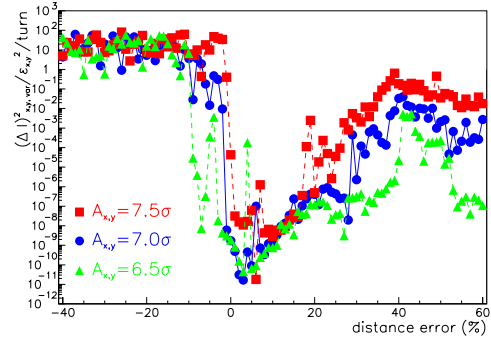


Figure 8: Variation of diffusion rate with wire position error at various amplitudes. Zero on the horizontal axis refers to a beam-wire distance of $(\theta_c/\theta_{x,y}^*)\sigma \approx 9.5\sigma$.

4 CONCLUSIONS

Weak-strong simulation studies show that at amplitudes between 6 and 8σ the wire compensation reduces the diffusion rate by many orders of magnitude. The tolerance to betatron phase errors is about 10° . The tolerable range of static strength errors extends between 0 and -10% . Transverse distance errors between 0 and 20% are acceptable. The most critical tolerance appears to be that to turn-to-turn fluctuation of the wire strength. Here a stability better than 0.1% must be achieved.

5 ACKNOWLEDGEMENTS

I thank O. Brüning, W. Herr, J-P. Koutchouk and F. Ruggerio for suggesting this study, support, helpful discussions, and a careful reading of the manuscript.

6 REFERENCES

- [1] T. Sen, et al., "Effect of the Beam-Beam Interactions on the Dynamic Aperture and Amplitude Growth in the LHC," CERN-SL-99-039 AP (1999).
- [2] Y. Papaphilippou and F. Zimmermann, "Weak-Strong Beam-Beam Simulations for the LHC," Proc. of the Workshop on Beam-Beam Effects in Large Hadron Colliders — LHC99, Geneva, April 12-17, CERN-SL-99-039 AP (1999) (J. Poole and F. Zimmermann eds.); published in Physical Review Special Topics – Accelerators and Beams 2, 104001 (1999).
- [3] H. Grote, et al., "LHC Dynamic Aperture at Collision," LHC Project Note 197 (1999).
- [4] J.-P. Koutchouk, "Principle of a Correction of the Long-Range Beam-Beam Effect in the LHC using Electromagnetic Lenses," LHC Project Note 223 (2000).
- [5] J.-P. Koutchouk, "Correction of the Long-Range Beam-Beam Effect in LHC using Electro-Magnetic Lenses," presented at IEEE PAC 2001 Chicago (2001).
- [6] J.-P. Koutchouk, these proceedings.
- [7] W. Herr, "Effects of PACMAND Bunches in the LHC," CERN-LHC-Project-Report-39 (1996).
- [8] J. Irwin, "Diffusive Losses from SSC Particle Bunches due to Long Range Beam-Beam Interactions," SSC-233 (1989).